

Temperature Distributions in Hollow Cathode Emitters *

Jay Polk and Colleen Marrese
Jet Propulsion Laboratory, M/S 125-109, 4800 Oak Grove Drive, Pasadena, CA 91109
(818) 354-9275, james.e.polk@jpl.nasa.gov

Ben Thornber
International Space University, Strasbourg, France

Lisa Dang
Northrup Grumman Space Technologies, Redondo Beach, CA

Lee Johnson
Jet Propulsion Laboratory, Pasadena, CA

AIAA-2004-4116 †

Life-limiting processes in hollow cathodes are determined largely by the temperature of the emitter. To support development of cathode life models we have developed a non-contact temperature measurement technique which employs a stepper motor-driven fiber optic probe. The probe is driven inside the hollow cathode and collects light radiated by the hot interior surface of the emitter. Ratio pyrometry is used determine the axial temperature profile. Thermocouples on the orifice plate provide measurements of the external temperature during cathode operation and are used to calibrate the pyrometer system in situ with a small oven enclosing the externally heated cathode. Initial measurements of the temperature distribution in a hollow cathode with the same geometry as a cathode that failed after operating at 12 A emission current for 27800 hours are discussed.

Introduction

Hollow cathodes used as thermionic electron sources in ion thrusters have demonstrated long life in space and in ground tests, but future missions have even more demanding life requirements. The emitter life is determined largely by the operating temperature, which has not been well-characterized. Lack of knowledge about the internal temperatures that drive the emitter failure modes results in large uncertainties in the achievable lifetime of hollow cathodes. In order to provide data for hollow cathode life models we have developed the capability to make accurate internal temperature measurements using a fast scanning fiber optic probe and a ratio pyrometer system.

The electron emitter of a conventional state-of-the-art hollow cathode is an impregnated porous tungsten tube (the insert) which is contained in a refractory metal tube with a plate containing a small orifice welded to the downstream end. The key to long insert life is to maintain a low temperature through the establishment of a layer of adsorbed oxygen and barium atoms that lowers the surface work function. In impregnated cathodes

†

*Copyright ©2004 by the American Institute of Aeronautics and Astronautics, Inc. The U.S. Government has a royalty-free license to exercise all rights under the copyright claimed herein for Governmental purposes. All other rights are reserved by the copyright owner.

†Presented at the 2004 Joint Propulsion Conference, Fort Lauderdale, FL, July 11-14, 2004.

Ba and BaO are supplied by barium calcium aluminate source material (the impregnant) incorporated in the pores of the tungsten. Gaseous Ba and BaO are released in interfacial reactions between the tungsten matrix and the impregnant, producing a temperature-dependent vapor pressure of these species inside the pores. The Ba and BaO then diffuse through the pores to the surface and replenish barium adsorbates lost by evaporation. The Ba and BaO transport rate through the pores depends on the vapor pressure of these species at the reaction front in the porous structure and the surface diffusion rate. Conventional cathodes are generally designed to operate with sufficient self-heating to guarantee that there is an adequate supply of Ba and BaO. This self-heating is accomplished by ion bombardment from the internal plasma in the insert interior and on the walls of the orifice.

Impregnated hollow cathodes have demonstrated over 16,000 hours of operation in a 30 cm diameter xenon ion engine on the Deep Space 1 (DS1) mission [1] and over 30,000 hours in a ground test of the DS1 flight spare engine [2]. One of the most important ground tests of a hollow cathode was conducted as part of the International Space Station Plasma Contactor development program [3, 4]. A cathode which was similar in design to those subsequently produced for the Space Station was tested at an emission current of 12 A for 27800 hours in a diode configuration with a planar anode mounted downstream. The xenon flow rate was initially 4.2 sccm, but was increased by the end of the test to 4.7 sccm to maintain stable operation in spot mode. Cathode orifice plate temperature was monitored during the entire test with a disappearing filament pyrometer and an infrared pyrometer and with a thermocouple for the first 6949 hours before it failed. The thermocouple indicated a temperature of approximately 1100°C, while the disappearing filament pyrometer yielded an average temperature of about 1260°C for the first 23776 hours. At that point the temperature increased rapidly to 1315°C and the required ignition voltage increased from approximately 50 V to over 725 V. After a total of 27795 hours the tip temperature exceeded 1350°C and the cathode would not ignite with the voltage available from the power supplies (1046 V). Post-test examination of the insert revealed a number of clues to the physical mechanisms of insert failure.

There are four main processes that degrade the barium adsorbate layer and can lead to insert failure [5]:

1. *Depletion of the barium source material.* The pores of conventional cathodes contain a limited amount of material which is eventually exhausted by vapor loss through the pores to the surface or tied up in barium tungstates and the stable monobarium aluminate that do not contribute to production of Ba vapor at typical operating temperatures.

2. *Insufficient production of Ba and BaO because of reaction product buildup at the interface between the impregnant and the tungsten matrix.* The reduction reaction that releases Ba proceeds by diffusion of reactants through this product layer. As it builds up over time, however, the diffusion rate drops. Unreacted source material may then become isolated by these product layers from the tungsten surfaces on which the reaction depends.

3. *Inadequate transport of Ba and BaO from impregnant deep in the matrix through the pores to the surface.* Conventional cathodes initially produce copious quantities of Ba and BaO. As the impregnant is consumed, however, the solid-vapor interface recedes into the pores. The vapor pressure for the given operating temperature is maintained at this interface, but the Ba and BaO must be transported through ever-increasing distances through the pores to the surface. The continually increasing conductance losses lead to reduced material flow through the pores or along the pore walls. When the supply rate drops below that required to balance losses from the surface, either the temperature must increase to compensate or the cathode fails to ignite. Increased operating temperature just accelerates the rate at which the supply is consumed.

4. *Closure of the surface pores by deposition of tungsten.* Tungsten crystals are often found on the downstream end of the insert emitter surface after long periods of operation [1, 5]. No insert failures have yet been attributed to this mass transport phenomenon, but these deposits could potentially close the pores that supply Ba and BaO in the emission zone. The tungsten is likely transported as tungsten oxide or tungsten

chloride (XXX?) vapor, which then dissociates in the plasma near the orifice or on the hottest surfaces at the downstream end of the emitter.

The insert temperature is the primary driver for the chemical processes and physical transport phenomena associated with these failure modes and a key indicator of cathode health, but is extremely difficult to measure. Contact temperature measurements on the interior are difficult because of the plasma environment and because they disturb the surface chemistry and electron emission processes. Optical access to the interior surface of the emitter is limited, making pyrometric measurements difficult. Most estimates of emitter temperature are based on thermocouple measurements of the exterior temperature. The temperature difference between these locations and the actual emitting surface are not known, however, and depend on the operating conditions and cathode thermal design. The life-limiting processes discussed above are exponentially dependent on the emitter temperature, so uncertainties in temperatures measured on the exterior limit their utility in assessing cathode life.

Salhi performed limited optical measurements of the internal temperature using a quartz fiber optic probe [6, 7]. The fiber was coated with a ceramic to protect it from the plasma and the probe end was cut at a 45° angle and coated with tantalum. This reflective coating acted as a mirror, directing light from a small hole in the ceramic coating on the side into the fiber. The probe was inserted and removed rapidly by hand before it melted, and light collected by the fiber as it scanned axially along the insert was measured with a SiGe sandwich detector sensitive to wavelengths between 400-1000nm and 1000-1800nm. This was a novel approach to gaining optical access, but suffered from several limitations. Determining the position of the fiber with any accuracy was impossible. The geometry of the probe tip resulted in collection of light from a relatively large area, limiting the spatial resolution. Contributions of plasma radiation to the collected signal were significant. Finally, the system was calibrated using a tungsten ribbon lamp, and no consideration was given to the effect of reflected light in the hollow cathode cavity or surface chemistry of the insert on the effective surface emittance.

The experiment described in this paper is designed to address these issues and provide reliable internal temperature measurements. Issues associated with plasma heating were avoided by using a high temperature sapphire fiber optic probe and a fast linear position system. Feedback from a rotary encoder on the actuator provides a position measurement resolution of .031 mm, while eliminating reflective coatings and relying on total internal reflection in the fiber yields a spatial resolution of about 2 mm. An optical system employing narrow bandpass interference filters eliminates plasma line radiation and measurement at two discrete wavelengths allows the use of ratio pyrometry to minimize sensitivity to variations in the distance of the probe to the surface. Finally, the system is calibrated in situ using the hollow cathode heater and thermocouples on the orifice plate, which automatically compensates for cavity and surface effects on the effective emittance.

This experiment is part of a major effort to develop models of hollow cathode wearout processes that can be used to guide the design of long-life hollow cathodes and assess their reliability for future deep space missions. The objective is to provide temperature profiles that can be used with cathode thermal models to understand the heat input distribution and to provide input data for models of barium depletion. This paper describes initial measurements made on a cathode with the same geometry as that tested in the Space Station Plasma Contactor wear test.

Test Apparatus

Cathode Assembly

The cathode used in these experiments is shown in Fig. (1). The insert is impregnated with barium oxide, calcium oxide, and alumina in the 4:1:1 molar ratios used in most conventional dispenser cathodes. A molybdenum ring and three equally spaced current leads are brazed to the upstream end of the insert. The

current leads were trimmed to a length of about 8 mm and bent out to contact the cathode tube inner wall. A swaged coaxial heater wrapped around the downstream end of the cathode was used to condition the emitter and to preheat it prior to ignition. Tantalum radiation shielding was wrapped around the heater coil to improve the heater efficiency. The cathode geometry is the same as that used in the Space Station Plasma Contactor wear test, but the heater design is slightly different. The heater diameter is approximately 30% smaller and the heater coil and radiation shielding are approximately 50% longer.

Figure 1: Cutaway diagram showing the cathode configuration and photograph of the assembly with the planar anode.

Two thermocouples were spot-welded to the edge of the cathode orifice plate, as shown in Fig. (1). Finer thermocouple wire was used than in the ISS plasma contactor wear test to minimize heat conduction from the orifice plate.

No keeper electrode was used in these tests. A flat molybdenum plate served as the anode. In initial experiments it was located 6 cm downstream of the cathode tip, as in the plasma contactor wear test. For the temperature measurements presented below, the anode was moved 1 cm further downstream to accommodate in situ calibration of the optical pyrometer system.

Vacuum System

The cathode assembly was mounted in a 1 m diameter by 2 m long vacuum facility. This chamber is pumped by one or two 25 cm diameter cryopumps. Pressure was monitored with a Granville Phillips Stabil Ion Gauge which was calibrated with xenon gas. The base pressure was typically 4×10^{-5} Pa (3×10^{-7} Torr) and the pressure during cathode operation ranged from 6.65×10^{-3} - 1.33×10^{-2} Pa (5×10^{-5} - 1×10^{-4} Torr).

Flow System

Xenon with a purity of 0.999995 was used as the cathode expellant. The flow rate was measured

with a Unit Instruments 1661 flow meter and controlled with an MKS 250C controller and XXX valve. The valve was mounted in the vacuum chamber so that all external feed lines were at above atmosphere pressure to eliminate the possibility of air leaks into the flow system. The meter was calibrated by flowing xenon into a known volume and measuring the rate of pressure rise with a precision pressure transducer, yielding flow rate measurements with an uncertainty of less than 2%. An Optomux data system with LabView control software was used for flow setpoint control and flow meter data logging.

Power Supplies

Heater and discharge power was provided by a XXX power supply and a XXX power supply, respectively, with the common returns grounded to the vacuum tank. The cathode was also grounded to the chamber through the mounting structure. Currents and voltages were measured to within 1% by the data system using calibrated shunts and voltage dividers.

Operating Conditions

The experimental setup was designed to reproduce the conditions of the Space Station Plasma Contactor wear test to the extent possible. The discharge voltage as a function of flow rate is shown in Fig. (2). With an anode-cathode spacing of 6 cm, the results are similar to those obtained in the wear test. The 7 cm anode-cathode spacing resulted in higher voltages for a given flow rate and transition from spot to plume mode operation at higher flow rates. The voltages and transition points were also sensitive to vacuum chamber pressure. These differences are due to changes in the potential distribution in the cathode-anode gap, and do not influence the internal cathode conditions significantly [8].

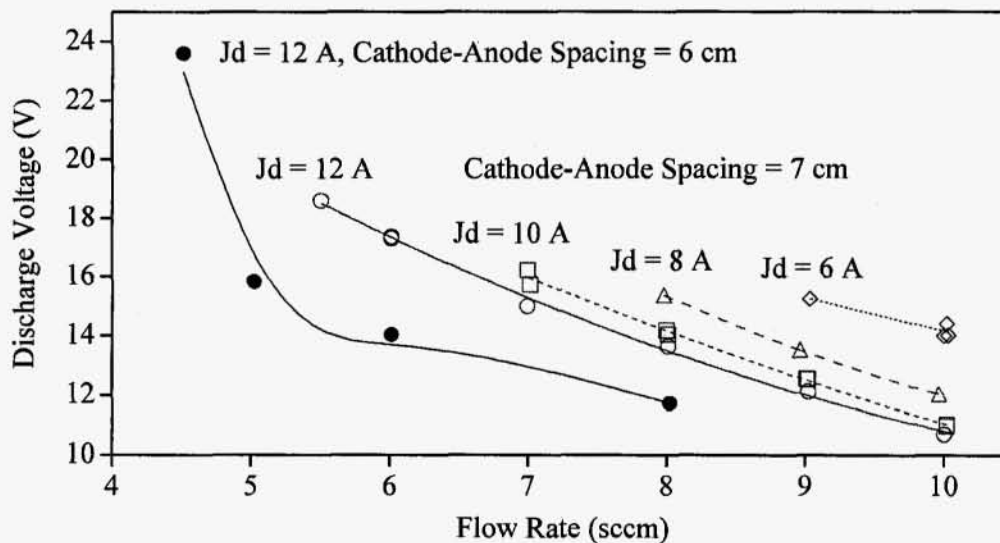


Figure 2: Discharge voltage variation with flow rate.

The orifice plate temperatures measured in this experiment with the two thermocouples are similar to those measured in the wear test with the disappearing filament pyrometer, but are considerably higher than

the thermocouple measurements from that test. The thermocouple used in the wear test may have had more thermal contact resistance [3]. Great care was taken in the experiments described below to ensure very good thermal contact by spot-welding the thermocouple beads directly to the orifice plate surface.

Insert temperature measurements were taken with discharge currents of 6-12 A and flow rates ranging from the onset of plume mode at each current level and 10 sccm.

Insert Temperature Probe

The challenges of making non-intrusive surface temperature measurements in a high temperature environment with a xenon plasma and barium metal vapor were overcome by using a high temperature fiber optic probe, a rapid scanning system to minimize probe heating and contamination, and ratio pyrometry at carefully selected wavelengths to eliminate interference from plasma radiation and source-detector geometry effects. Each of these elements is described below.

Fiber Optic Probe

Light from the interior surface of the insert was collected with a 425 micron diameter sapphire fiber. The end of the fiber was cut and polished at a 45° angle to the fiber axis, which bends the acceptance cone by 90°. The fiber field of view is therefore sideways, and it collects light from a region about 2 mm in axial extent and 180° laterally. As shown schematically in Fig. (3), the probe is located inside a gas plenum upstream of the cathode. The fiber is terminated with a standard SMA connector and is attached to a fiber optic feedthrough at the upstream end of a bellows, which allows probe motion parallel to the axis of the cathode. The probe is carefully positioned to scan along the interior of the cathode approximately 0.5-1 mm from the insert surface. It is normally parked upstream of the cathode and is driven downstream by the positioning system a total distance of 52 mm, which brings the tip within 1.7 mm of the upstream surface of the orifice plate.

Motion Control System

The probe is moved with a fast, stepper motor-driven positioning system located outside the chamber. Another bellows feedthrough on the chamber forms the vacuum seal, as shown in Figs. (4) and (5). The peak speed of the linear positioning system is 350 mm/s, and with a programmed acceleration and deceleration profile at the start and endpoints the probe travels in and out of the cathode in about 400 msec. The probe location is monitored with .032 mm resolution using a rotary encoder. Lateral motion of the fiber is prevented using two fiber guides upstream of the cathode. A flexible fiber optic cable transmits the light signal from the moveable stage inside the vacuum chamber to a fiber optic feedthrough on the chamber door.

Ratio Pyrometer System

The signal is transmitted from the chamber to the optics system shown in Figs. (6) and (7) with another flexible fiber optic cable. Light exiting the fiber is collimated onto a long wave pass dichroic beam splitter. The beamsplitter transmits wavelengths around 1500 nm with an efficiency of 85% and reflects shorter wavelengths around 1260 nm with 97% efficiency. The reflected and transmitted beams are filtered using interference filters with a 10 nm bandpass centered on 1200 and 1500 nm, then focused onto Hamamatsu InGaAs photodiodes. These wavelengths were chosen to give good spectral separation for ratio pyrometry and because there is no interfering xenon line radiation.

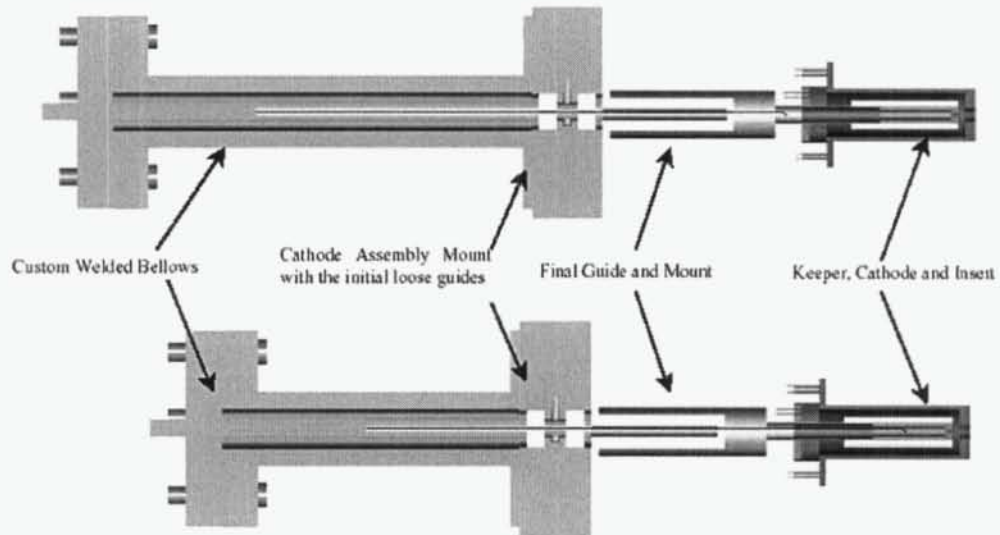


Figure 3: Schematic of the scanning fiber optic insert temperature probe.

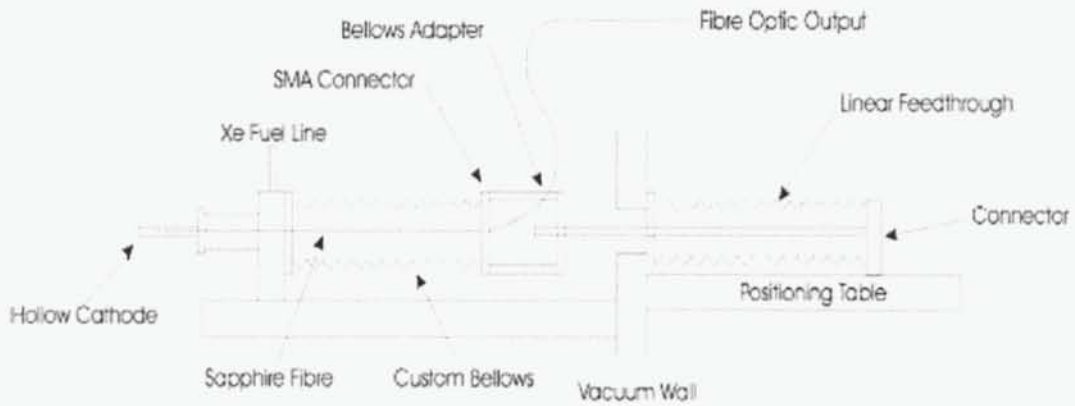


Figure 4: Schematic of the fiber optic probe motion system.

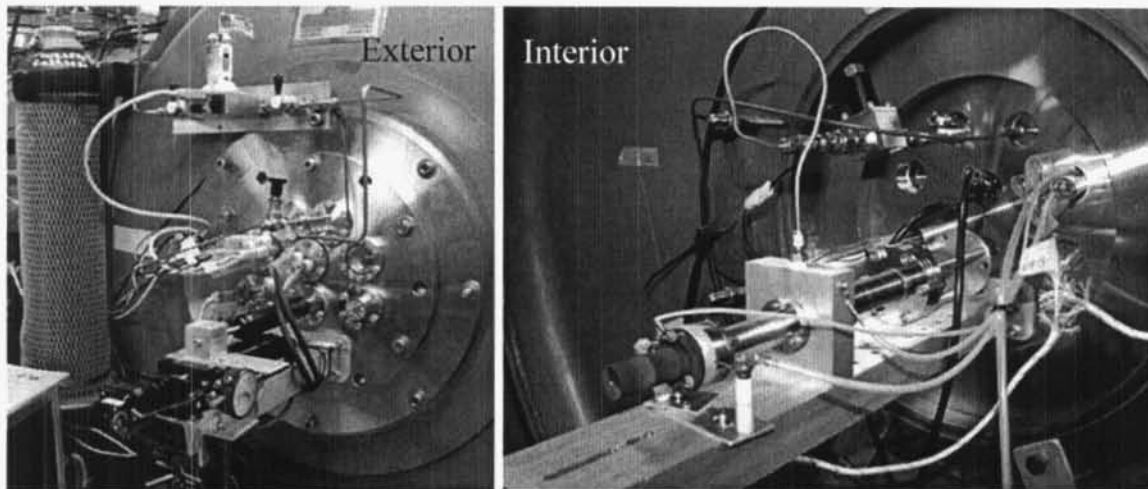


Figure 5: Photographs of the probe actuator system.

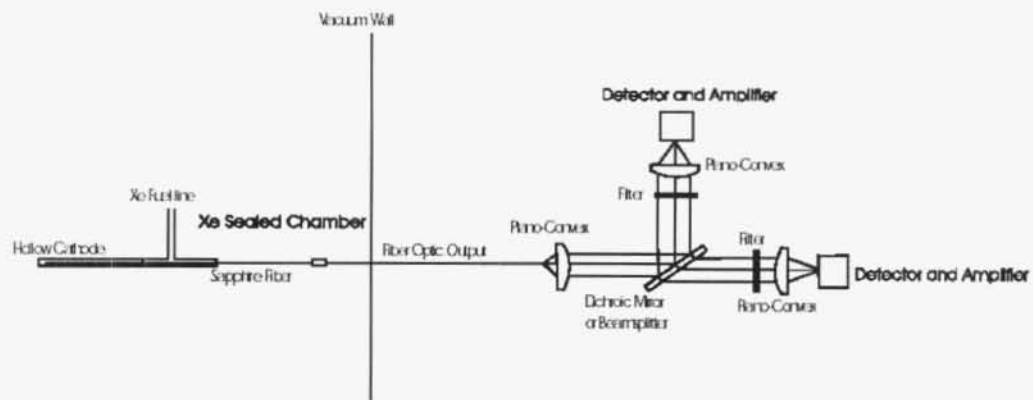


Figure 6: Schematic of the 2-color pyrometer system.

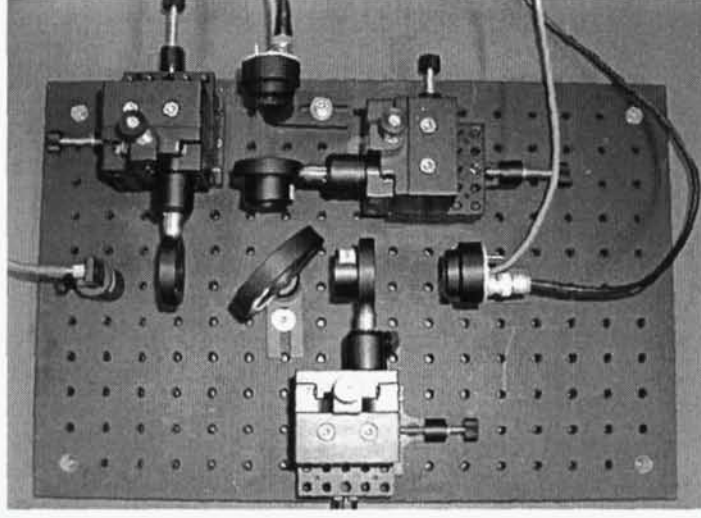


Figure 7: Photograph of the 2-color pyrometer system.

The voltage signals from amplifiers in the photodiode assemblies are collected with a data acquisition system. The output from the rotary encoder on the positioning system is used to time the data acquisition, so the photodiode signals are perfectly coordinated with the motion. The voltage output from photodiode i , $V_{out,i}$, is given by the expression

$$V_{out,i} = V_{0,i} - G_{t,i}R(\lambda_i)\tau_o(\lambda_i)\tau_f(\lambda_i)\epsilon(\lambda_i)F_g\Delta\lambda_{f,i}L_{\lambda,b}(\lambda_i, T) \quad (1)$$

where $V_{0,i}$ is the voltage offset of amplifier i (signal with no illumination), $G_{t,i}$ is the transimpedance gain of the internal amplifier (V/A), R is the responsivity of the detector (A/W), τ_o is the transmission of the optics system, τ_f is the fiber transmission, ϵ is the effective surface emittance, and $\Delta\lambda_{f,i}$ is the bandpass of interference filter i , which is centered on the wavelength λ_i . F_g is a geometric factor which is a function of the distance of the fiber from the surface and the acceptance angle, but not the wavelength. The spectral radiance, $L_{\lambda,b}(\lambda_i, T)$ is approximated well in this wavelength and temperature range by the Wien formula:

$$L_{\lambda,b}(\lambda_i, T) = \frac{c_1}{\lambda_i^5} \exp(-c_2/\lambda_i T), \quad (2)$$

where T is the surface temperature and c_1 and c_2 are constants. The fiber optic probe also collects light from other surfaces in the hollow cathode interior which is reflected off of the surface in the field of view. This is accounted for in the effective emittance, which is expected to be near unity because the insert forms a cavity approximating a black body. The ratio of the diode voltages is

$$\frac{V_{out,1}}{V_{out,2}} = \frac{R(\lambda_1)\tau_o(\lambda_1)\tau_f(\lambda_1)\epsilon(\lambda_1)\lambda_2^5\Delta\lambda_{f,1}}{R(\lambda_2)\tau_o(\lambda_2)\tau_f(\lambda_2)\epsilon(\lambda_2)\lambda_1^5\Delta\lambda_{f,2}} \exp\left[\frac{c_2}{T}\left(\frac{1}{\lambda_2} - \frac{1}{\lambda_1}\right)\right] = C_1(\lambda_1, \lambda_2) \exp\left(\frac{C_2(\lambda_1, \lambda_2)}{T}\right). \quad (3)$$

where C_1 contains the ratio of detector responsivities and optical system transmission at the two wavelengths, the ratio of wavelengths, the ratio of filter widths and the ratio of effective emittances. It depends explicitly on the values of the two wavelengths, but the only temperature dependence is that of the ratio of effective emittances. One primary advantage of the ratio technique is that the geometric factor F_g cancels

out, so the ratio is insensitive to variations in the fiber-to-surface distance. C_2 depends only on physical constants and the two wavelengths. For the wavelengths chosen for this system, $C_2 = 2397$ K.

Calibration

The pyrometer response was calibrated in situ using the cathode heater. A small cylindrical oven consisting of tantalum radiation shields can be slipped over the cathode using a motion feedthrough in the vacuum chamber door. This oven provides a nearly isothermal region at downstream end of the cathode, so the pyrometer signal there can be related to the temperatures measured with the thermocouples on the orifice plate. Figure (8) shows the two photodiode signals. There is a large gradient upstream of the insert due to axial conduction and radiation losses from the unshielded portion of the cathode tube. Inside the oven, however, the gradient is much smaller and the signals are almost constant for the last 10 mm at the downstream end.

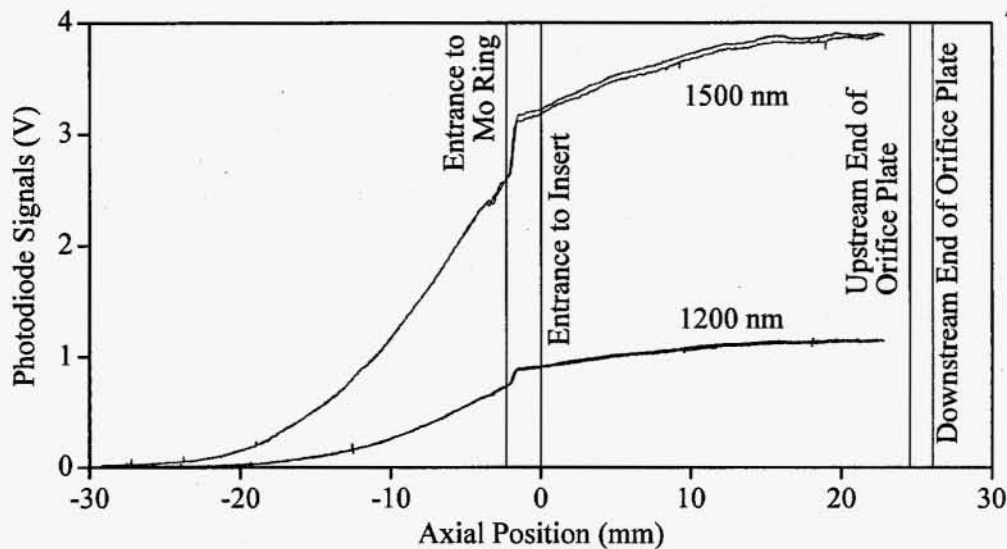


Figure 8: Typical photodiode voltage signals with the calibration oven.

Figure (9) shows the ratio of photodiode voltages from Fig. (8) in the insert region. Similar curves were obtained for a range of heater powers. The photodiode voltages were extrapolated to the orifice plate and plotted as a function of the orifice plate temperature measured with the thermocouples, as shown in Fig. (9). The two thermocouples agree within 2°C when the calibration oven is in place. The photodiode signals are very repeatable from scan to scan, but exhibit a slow monotonic decay over many scans, as shown in Fig. (10). Examination of used fibers with energy dispersive spectroscopy in a scanning electron microscope revealed barium on the surface. This coating, which comes from barium vapor in the insert plasma, slowly degrades the fiber transmission. Calibrations must therefore be performed frequently to monitor the drift in response.

Seven calibration curves measured while taking the data presented in the next section are shown in Fig. (11). They are plotted in the functional form $\ln(V_{out,1}/V_{out,2}) = \ln C_1 + C_2/T$ based on Eq. (3). The data are linear, as expected. The slope varies from 2490-2606, which is 4-8/ μs dependent on temperature.

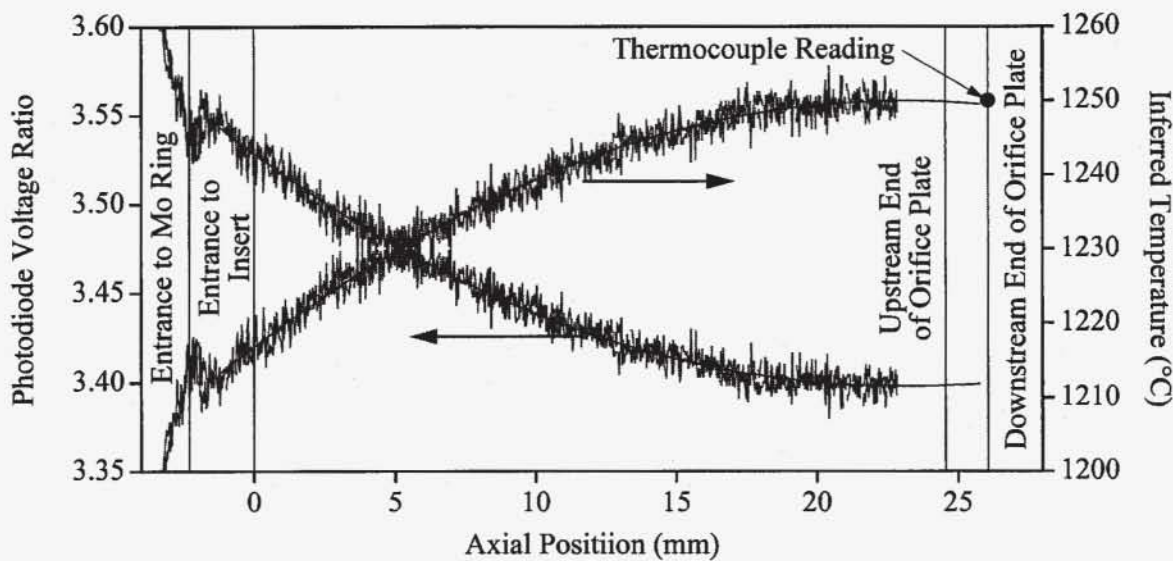


Figure 9: Ratio of photodiode voltages with the calibration oven. Temperatures inferred from the ratio curve and the calibration data show that the temperature is uniform over about 10 mm at the downstream end of the insert.

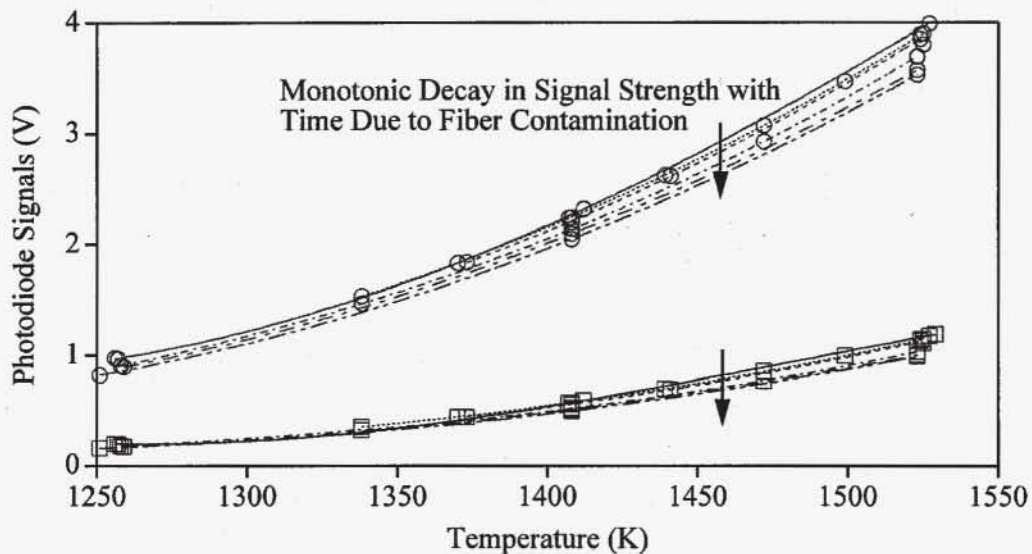


Figure 10: Variation in peak photodiode voltages with temperature. Slow decay in signal with time is caused by contamination of the fiber optic probe with barium.

This is probably related to small changes in the effective emittance ratio with temperature. The decay in signal strength due to barium contamination causes a shift in the calibration curve. The changes are gradual, with the exception of one episodic shift associated with operation at low flow which caused a transition to plume mode and discharge extinction. The small changes in the calibration yield differences in

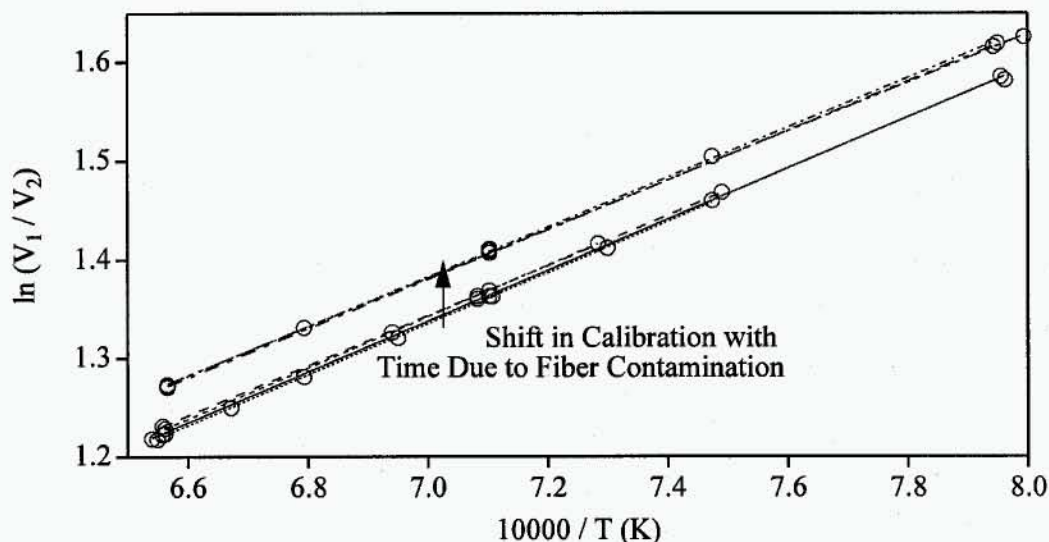


Figure 11: Typical calibration curves. Shifts in calibration are due to probe contamination.

the calculated temperature of only 2-3°C. The large shift results in calculated temperature differences of up to 30°C if applied to data taken before the shift. However, three operating points that were repeated after the major shift agreed with earlier measurements to within 2-5°C when the proper calibration was used, demonstrating that the technique is reliable if calibrations are performed often.

Operating Procedures

Data presented below were obtained after about 33 hours of cumulative operation on a new cathode insert. Preliminary measurements with the probe and with the orifice plate thermocouples in the first few hours of operation indicated much higher temperatures (XXX°C). Large changes in temperatures measured with thermocouples on the exterior have also been observed in extended duration tests [?], and are apparently associated with initial cathode activation. Data obtained here are representative of cathode operation after the large initial transient, but the cathode insert may not yet have reached true equilibrium.

The operating procedure was designed to obtain insert temperature measurements over a range of conditions and monitor any changes in the pyrometer system calibration. An initial calibration was performed with the oven. The cathode was then ignited at a particular discharge current level and the discharge voltage and thermocouple readings were allowed to stabilize to within XXX V and 2°C, respectively. The insert temperature was measured with the fiber optic probe, then the flow rate was changed and the process was repeated. The calibration was repeated after every current level (every 3-7 scans). Extensive testing demonstrated that the measurements are repeatable at a given operating point to within 1-2°C, so generally only one scan was obtained at each setting to minimize fiber contamination. Some points were repeated over long pe-

riods of time to check long-term repeatability, as noted above. The data were analyzed using the calibration curve taken before that dataset if the subsequent calibration indicated no major shifts in response.

Results

The temperature distribution measured at 12 A and 5.5 sccm is shown in Fig. (12) with a fourth order polynomial fit. The residuals plotted above this curve show the noise typically observed for this temperature range. The standard deviation in these measurements is about 3.5 °C and is dominated by a slight hysteresis. The curve fit is used to extrapolate 1.7 mm downstream to the temperature peak at the end of the insert. The temperatures measured with the thermocouples are also shown in Fig. (12). Under nearly isothermal conditions with the cathode enclosed in the radiation shields during calibration measurements, the thermocouple readings agreed to within 2°C. During cathode operation, however, they differed by 10-15 °C, indicating small variations in temperature near the tip.

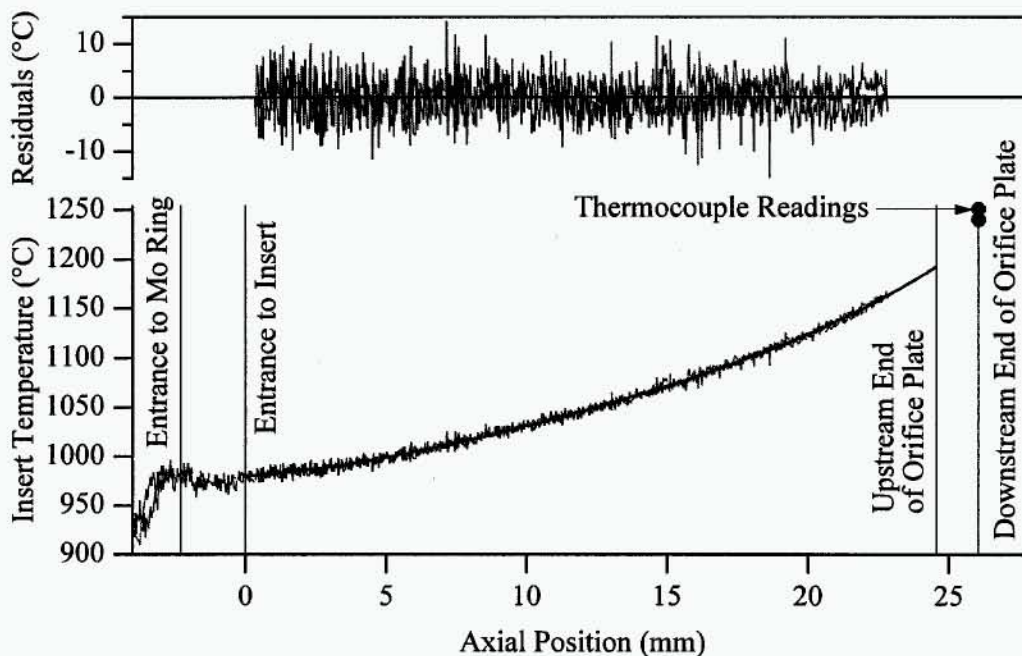


Figure 12: Typical temperature distribution measurement and curve fit, showing extrapolation downstream to estimate peak temperature.

Insert temperature distributions and peak orifice plate temperatures for currents of 6, 8, 10 and 12 A are shown in Fig. (13). The flow rates for these measurements were 9, 8, 7 and 5.5 sccm, respectively. These values are within 0.5 sccm of the minimum flow rate for spot mode operation under these conditions. The temperature rises monotonically toward the downstream end of the insert and increases by approximately 50 °C with every 2 A increase in current. The peak insert temperatures are all less than the orifice plate temperatures.

A slight, but reproducible, variation in the temperature distribution with flow rate was observed at all current levels. For example, Fig. (14) shows the curve fits to data obtained at 12 A. In all cases the temperature decreased slightly with increasing flow rate. This is also shown in Fig. (15), which plots the

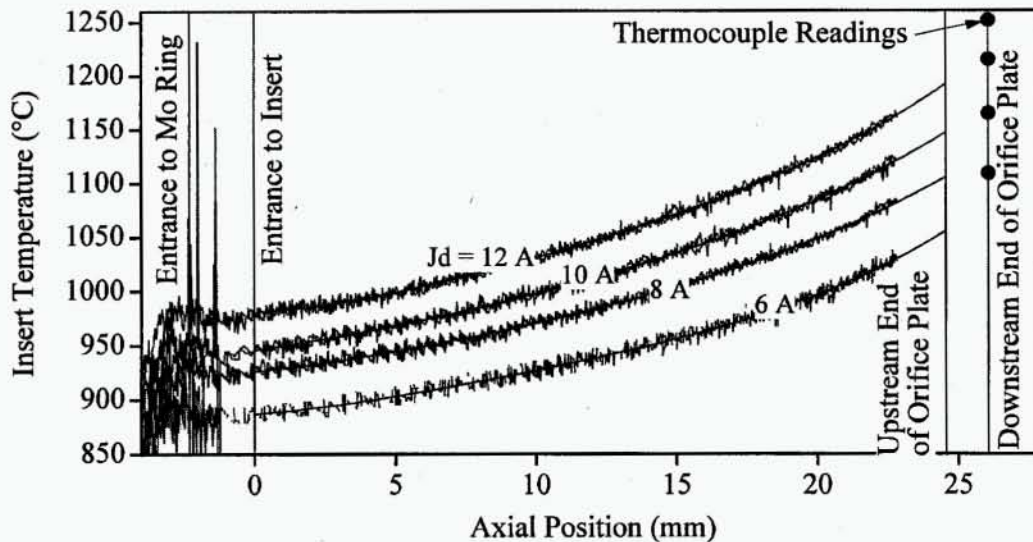


Figure 13: Variation in temperature distribution with discharge current level for the minimum flow rates tested at each current; 9, 8, 7 and 5.5 sccm for 6, 8, 10 and 12, respectively.

peak insert and orifice plate temperatures as a function of flow rate and current level. In contrast to the insert temperature, the orifice plate temperature increases slightly with increasing flow. The difference between the peak insert temperature and the orifice temperature for this range of currents and flow rates is plotted in Fig. (16). The difference varies between 50 and 90 °C and increases with both flow rate and current. The orifice plate temperature is largely controlled by heat dissipation in the orifice, which increases with current and flow rate.

Conclusions

This dataset represents the first comprehensive characterization of the temperature distribution on the actual emitting surface of a hollow cathode. This product was enabled by the development of a robust, non-intrusive scanning fiber optic probe technique. The results of initial measurements on a cathode with the same geometry as that used in the Space Station Plasma Contactor wear test demonstrate that the axial temperature profile increases monotonically along the insert by 170-200°C with peak temperatures of 1050-1180°C for discharge currents of 6-12 A. The temperature increases significantly with discharge current (approximately 50°C for each 2 A increase in current) and shows a weak dependence on flow rate. For this range of operating conditions and orifice geometry, the insert temperature was less than the orifice plate temperature by 50-90°C. The results indicate that the orifice plate temperature is determined largely by orifice heating, which scales with current and flow rate. The insert temperature for this cathode geometry is influenced by conduction from the hot orifice plate as well as direct heat inputs from the plasma.

The insert temperature determines the reduction and decomposition chemistry that produces barium and barium oxide vapor in the pores, the transport of barium to the surface, loss of barium by desorption and formation of volatile tungsten compounds that may be responsible for tungsten crystal growth in the insert. Temperature is the key driver for all of the important mechanisms controlling insert life. Additional

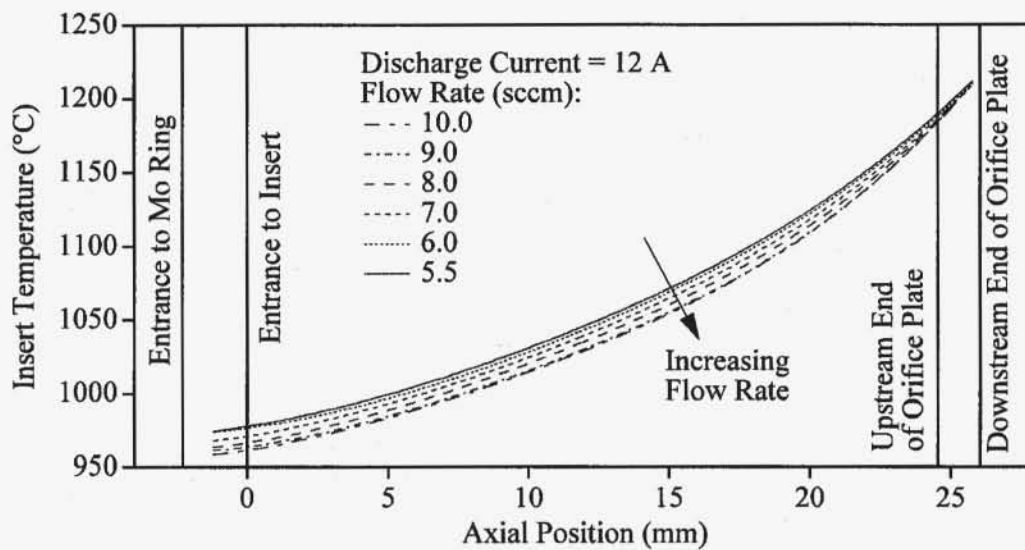


Figure 14: Variation in insert temperature distribution with flow rate for a discharge current of 12 A.

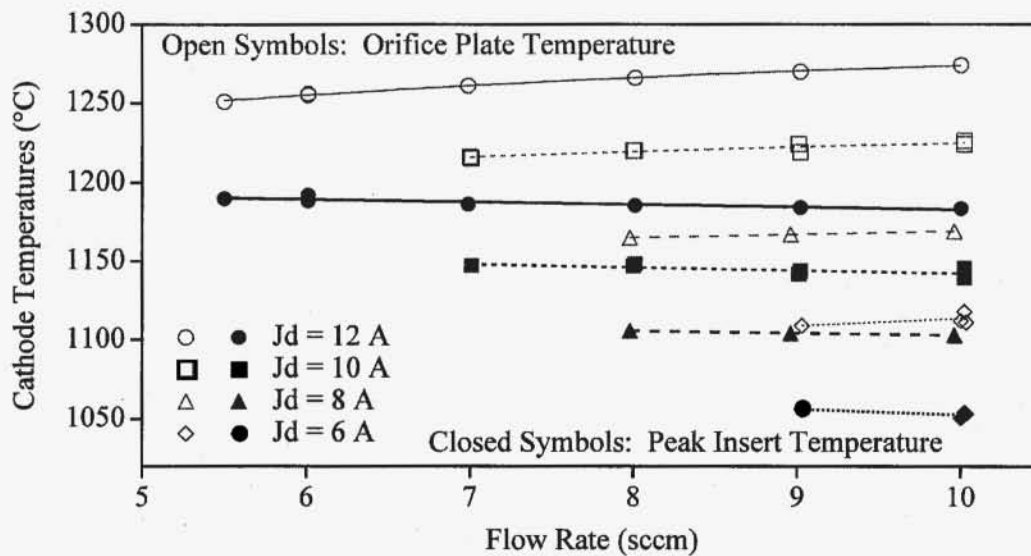


Figure 15: Variation in peak insert and orifice plate temperatures with current and flow rate.

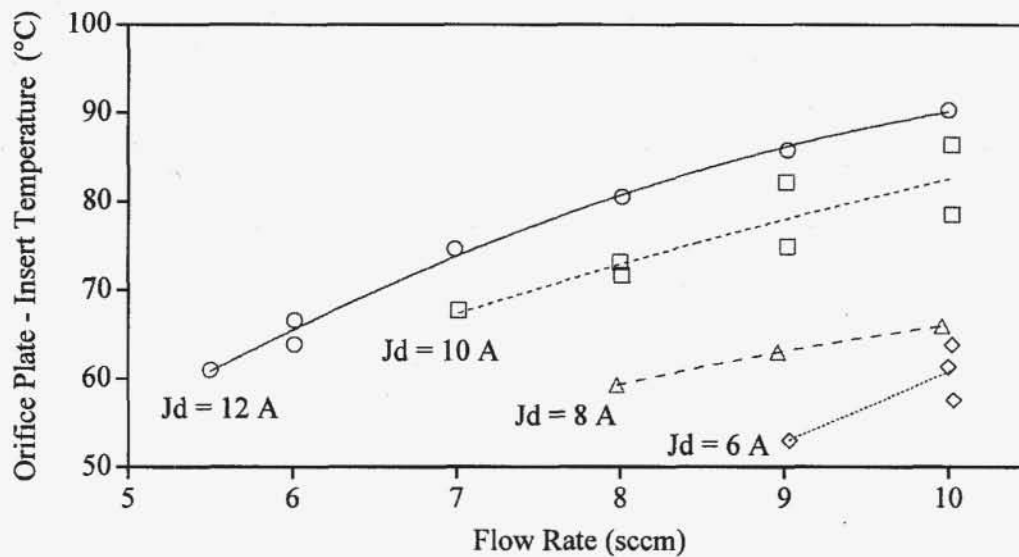


Figure 16: Difference between peak insert and orifice plate temperatures as a function of current and flow rate.

measurements on cathodes with different orifice and insert sizes will be collected to characterize the effect of geometry on the temperature distribution. The results will be used to benchmark thermal models to gain insight on the distribution of heat loads between insert and orifice plate. Determining how strongly coupled the two components are will provide a valuable cathode design tool. In addition, the distribution of plasma density, potential and electron temperature will be measured for this cathode geometry using a fast scanning Langmuir probe [8]. With these data we can estimate the surface electric field, determine the reduction in work function by the Schottky effect, and calculate the thermionic electron emission current density. This will give a complete picture of the cathode emission processes. The temperature data will be used in models of barium depletion [9] and the insert plasma [10] to calculate cathode insert life. Detailed characterization of the emitter temperature is a critical tool in the program to develop a thorough understanding of cathode emission and life-limiting processes.

Acknowledgements

The research described in this paper was carried out by the Jet Propulsion Laboratory, California Institute of Technology, under a contract with the National Aeronautics and Space Administration in support of Project Prometheus.

References

- [1] J.E. Polk, D. Brinza, R.Y. Kakuda, J.R. Brophy, I. Katz, J.R. Anderson, V.K. Rawlin, M.J. Patterson, J. Sovey, and J. Hamley. Demonstration of the NSTAR Ion Propulsion System on the Deep Space One Mission. In *27th International Electric Propulsion Conference*, Pasadena, CA, 2001. IEPC-01-075.

- [2] A. Sengupta, J.R. Brophy, and K.D. Goodfellow. Status of the Extended Life Test of the Deep Space 1 Flight Spare Ion Engine after 25,700 Hours of Operation. In *39th Joint Propulsion Conference*, Huntsville, AL, 2003. AIAA-2003-4558.
- [3] T. Sarver-Verhey. Continuing Life Test of a Xenon Hollow Cathode for a Space Plasma Contactor. In *30th Joint Propulsion Conference*, Indianapolis, 1994. AIAA-94-3312.
- [4] T.R. Sarver-Verhey. 28,000 Hour Xenon Hollow Cathode Life Test Results. In *25th International Electric Propulsion Conference*, Cleveland, OH, 1997. IEPC 97-168.
- [5] T.R. Sarver-Verhey. Destructive Evaluation of a Xenon Hollow Cathode After a 28,000 Hour Life Test. In *34rd Joint Propulsion Conference*, Cleveland, OH, 1998. AIAA-98-3482.
- [6] A. Salhi, R.M. Myers, and P.J. Turchi. Experimental Investigation of a Hollow Cathode Discharge. In *23rd International Electric Propulsion Conference*, Seattle, WA, 1993. AIAA-93-XXX.
- [7] A. Salhi. *Theoretical and Experimental Studies of Orificed, Hollow Cathode Operation*. PhD thesis, The Ohio State University, Ohio, 1993.
- [8] D.M. Goebel, K.K. Jameson, R.M. Watkins, and I. Katz. Hollow Cathode and Keeper-Region Plasma Measurements Using Ultra-Fast Miniature Scanning Probes. In *40th Joint Propulsion Conference*, Fort Lauderdale, FL, 2004. AIAA-2004-3430.
- [9] I. Katz, J. Anderson, D.M. Goebel, R. Wirz, and A. Sengupta. Plasma Generation Near an Ion Engine Discharge Chamber Hollow Cathode. In *39th Joint Propulsion Conference*, Huntsville, AL, 2003. AIAA-2003-5161.
- [10] I. Mikellides, I. Katz, D. Goebel, and J. Polk. Theoretical Model of Hollow Cathode Insert. In *40th Joint Propulsion Conference*, Fort Lauderdale, FL, 2004. AIAA-2004-3817.

End of File

